

# Beam Bundle Model of Human-Like Fingertip for Investigation of Tactile Mechanism

Van Anh Ho, Zhongkui Wang, and Shinichi Hirai  
Department of Robotics  
Ritsumeikan University  
525-8577 Kusatsu Shiga, Japan

**Abstract**— We have proposed a **Beam Bundle Model** for modeling of a human fingertip during pushing and sliding action with friction, especially stick-to-slip transition, to overcome mentioned issues. In order to construct its three-dimensional non-homogeneous structure, we took sequence of magnetic resonant images, which bring consecutive cross-sectional layers of the human fingertip with distribution of skin, tissue, bone, and nail. Simulation results show a twofold aspect. Firstly, it can generate not only normal force distribution caused by pushing, but also response of friction force during sliding. Secondly, and more interestingly, the model dynamically produces localized displacement phenomenon on the contact area during stick-to-slip phase, which indicates how slippage *erodes* the contact area before the total slippage of the fingertip occurs. Finally, we investigated role of sliding mechanism acting on human fingertips' contact area in stable lifting of an object, in order to show the potential of the model in studying tactile mechanism of human and apply to robotic systems.

## I. INTRODUCTION

Never in the past had human use touching/sliding action of fingertip as in the present, thanks to smart devices. Also, interaction between human fingertips and machines requires a novel sensing system to be able to detect diverse actions, such as pushing, squeezing, and especially sliding. Back to the state of the art, among many senses, tactile perception is considered to as one of the most important factors for both humans and robots, which permits acquisition of the outside world information, especially the grasped object's characteristics for stable/dexterous manipulation [1]. In the virtual world of a haptic system, it has been shown that in order to assure a successful tactile exploration, it is indispensable to create a significant *sensation* of realness on the user through virtual objects [2].

Model of bio-mimetically structured fingertip has been an interesting issue in field of robotics for years. It starts with homogeneous soft fingertip model, in which fingertips possess simple geometrical shapes, such as cylindrical or hemispherical ones. Xydas *et al.* [3] constructed a nonlinear finite element analysis (FEA) to study contact mechanics of a hemispherical fingertip. They mostly focused on normal contact that causes a pressure distribution profile over the contact zone in order to verify power-law theory in material mechanics. A three dimensional FE models of human and monkey fingertips with five layers of epidermis, dermis, and bone had been developed to investigate roles of epidermis layer, as well as other layers' stiffness, in representation of

a line load on the fingertip [4]. The model perfectly fitted to experimental data. Nonetheless this model, even reduced, costs abundant time for calculation. In addition, this model had ignored friction, as well as dynamic response during sliding motion. More complicated model of human fingertip with accurate geometries was proposed in [5]-[7] to study sole deformation of the fingertip on a flat plate. Above research, however, only addressed static models to predict stress-strain during making contact; neither of them could reappear dynamic change of stress-strain in time domain.

Sliding action is of crucial factors that a fingertip must feel and act correspondingly in order to prevent it in grasping or manipulation. Kao and Cutkosky [8] built a closed form for modeling manipulation with sliding fingers. However, this research was limited to quasi-static simulation and homogeneous fingertips, while could not help to assess details of slippage on the contact area. Konyo *et al.* [9] has investigated human fingertip under vibro-tactile stimuli in order to represent force in a haptic display system. A dynamic model of a human fingertip was proposed to study stick/slip events on the contact surface while suffering external high-frequency stimuli. Nonetheless, this model only comprised of a mass connected with a spring and a damper that arranged in parallel, which is insufficient for a complicatedly structured human fingertip. Recently, Nahvi *et al.* [2] has introduced a friction display system for virtual environment with a simplified model of a virtual spring during transition from slip to stick, and vice versa. While this model can extract human fingertip's characteristics such as switching between stick and slip, oscillation in slip phase; it cannot clarify how partial slips occur on the contact area during stick phase that is, as stated by authors, crucial to assess slip perception.

In this research, we applied **Beam Bundle Model** (BBM) into modeling a human fingertip. Magnetic Resonant images (MRI) of one volunteering subject's index fingertip were utilized to construct a mathematical model of the fingertip's structure. We first characterize pre-sliding regime on a real human finger to find out its inherent characteristics. We afterward simulated the model with considered issues, and we succeeded in representation of localized displacements (also referred to as skin local stretch) during pre-slide phase of the fingertip, which is considered crucial to assess stick/slip events on the contact pad. This work can be utilized not only in haptic sensation, but also in development of sensors for

detection of slippage.

## II. BEAM BUNDLE MODEL OF HUMAN FINGERTIP

### A. Previous Model of a Robotic Soft Fingertip

Previously, we proposed a model to simulate deformations of hemispherical soft fingertips [10]. In this model, the soft fingertip is necessarily elastic and homogeneous with pre-determined geometrical shape. Deformation of the fingertip under normal and tangential loads were modeled through *virtual* elastic compressible and bendable cantilevers. The contact area was meshed with viscoelastic model according to finite element theory. Using this model, authors were able to simulate the sliding motion, and observe responses of normal force and friction force. Moreover, simulation also produced stick/slip on the contact area, helping us to assess how and when the slippage occurred on the contact surface. Nonetheless, this model is not sufficient in modeling non-homogeneous, non-elastic fingertips with irregular geometrical shape. Also, we ignored dynamic response of normal force during load/unload phase.

### B. Construction of Human Fingertip Using MR Images

In order to accurately measure the 3D internal and external geometries of human fingertip, a 3 Tesla MRI system is used in our experiments. Cross-sectional MR images of an index finger were collected with a volunteering 25-year-old adult male, having no history of finger disease. A total of 32 images with size of  $120 \times 120 \text{ mm}^2$ , 1.2 mm slice thickness and  $512 \times 512$  matrices (pixel size of  $0.23 \times 0.23 \times 1.2 \text{ mm}^3$ ) were acquired using a fast gradient echo (fgr) sequence with 9.8 ms repetition time (TR), 4.2 ms echo time (TE) and 30 flip angle. These images were obtained representing volume of the fingertip in term of consecutive cross-sectional layers. For each image, we can observe the distribution of layers such as skin, tissue, bone, and nail position as illustrated in Fig. 1.

It is necessary to assess the exact distribution of constructed layers of the fingertip. We utilized image processing functions in OpenCV to extract boundaries of skin, bone, and the nail. Note that since MR signal is mainly derived from protons of water molecules in body tissues, we were not able to extract shape of the nail that is dry, but only boundary on which the nail is placed on. Each boundary was formed by a group of points which were afterward interpolated into a curve (see Fig. 2(a)). As a result, for each image, we were able to collect four fitted curves, including for skin, lower bone, upper bone, and nail as illustrated in Fig. 2(a). By repeating this process on all images, three-dimensional geometrical shape of the fingertip could be constructed.

### C. Construction of BBM for Human Fingertip

After obtaining boundary curvatures of the human fingertip structure, we need to fill in the remained volume with *virtual beams*, which are similar to elastic cantilever aforementioned in [10]. These beams have two ends constrained by an upper bound (nail) and a lower bound (skin). Each virtual beam possesses cylindrical shape with geometrical

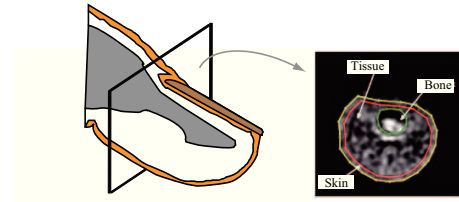


Fig. 1. MR images of consecutive cross-sectional layers of a human fingertip, showing the distribution of skin, phalanx, and nail.

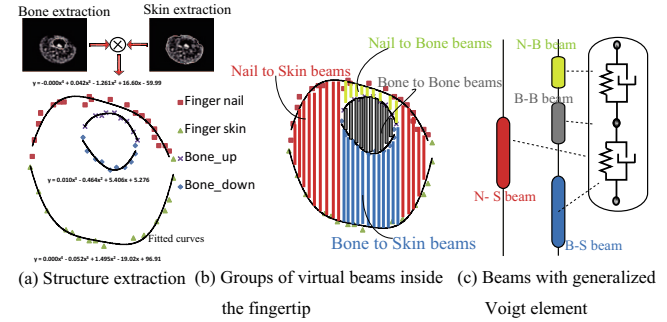


Fig. 2. Structure of human fingertip from MRI.

property, such as height, predetermined based on known fitted curves of nail, bone, and skin. Since layers of MR images have a pitch of 1.2 mm along the volume of the fingertip as mentioned in the above section, and in order to fill in beams to fit nicely to the fingertip's volume, each beam has a cross-sectional area's diameter of 1.2 mm. As a result, distance between basic axes of two neighboring beams is also specified as 1.2 mm.

In order to reflect relaxation of normal force mentioned in [3], we assigned each beam with a *generalized Voigt* model that consisting of two Voigt elements, each element has viscoelasticity characterized by a spring and a damper connected in parallel. After filling in with virtual beams, as illustrated in Fig. 2(b), there are two main groups of beams, including beams attach to nail and skin (N-S) and beams attach to nail through bone (N-B-S). Beams in the latter group are constituted by three separated beams connected in series: N-B, B-B, and B-S as shown in Fig. 2(c). As a result, virtual beams are not necessarily homogeneous as in [10]. By using this proposal of inhomogeneous beams, we could fill in *any* complicatedly-structured soft fingertip.

Supposed that the fingertip was pushed vertically onto a rigid flat surface, causing a set of contact boundary points on skin. We then meshed the contact area (or skin) utilizing finite element analysis, covered the contact area with a set of triangles (Fig. 3(a)); in which stress-strain relationship of each triangle is represented by a Voigt element consisting of a spring and a damper connected in parallel (Fig. 3(b)). Each triangle has three nodes attached to three corresponding free-ends of three beams that belong to either N-S or B-S group (see Fig. 3(c)). There exists two types of contribution of beams on one triangle: partly covering, and superposition. The former occurs more often than the latter case, causing

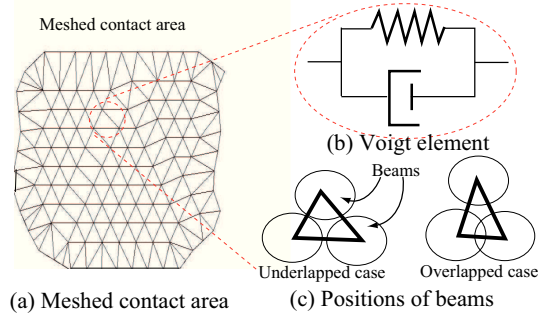


Fig. 3. Meshed contact area.

coverage ratio of entire contact area is always less than 100%. The coverage varies depending on how coarse or fine we meshed the contact area, and the maximum ratio that has been reached with less superposition is 96%. As a result, we can flexibly change the coverage ratio by varying beams' geometrical shape to adapt to specific simulation.

Thus, beams are constrained on the contact area on the skin; and the movement of beams's free-ends would be helpful to assess stick/slip events on the contact area during sliding motion. We have named this model as Beam Bundle Model (BBM).

#### D. Derivation of Motion Equation

1) *During Loading/Unloading*: In this section, we derive general equation for obtaining normal deformation of one inhomogeneous beam constituted by a set of Voigt models connected in serial, which is referred to as generalized Voigt model.

Supposing that one beam consists of  $n$  Voigt elements, let us define  $\varepsilon$  be the extensional strain of the beam while  $\varepsilon_i$  be the extensional strains of the  $i$ -th element. Extensions  $\varepsilon$  and  $\varepsilon_i$  through  $\varepsilon_{n-1}$  are independent state variables, and  $\varepsilon_n$  can be described dependently by other variables as follows:

$$\varepsilon_n = \varepsilon - \varepsilon_1 - \dots - \varepsilon_{n-1}. \quad (1)$$

Let  $E_i$  and  $c_i$  be the elastic and viscous moduli of the  $i$ -th Voigt element. Noting that stresses generated by individual elements are equal to each other, we have:

$$\sigma = E_1 \varepsilon_1 + c_1 \dot{\varepsilon}_1 = E_2 \varepsilon_2 + c_2 \dot{\varepsilon}_2 \dots = E_n \varepsilon_n + c_n \dot{\varepsilon}, \quad (2)$$

where  $\sigma$  indicates the generated stress by the deformation of the beam. Dividing the above equations by  $c_1$  through  $c_n$  and summing up all equations yields:

$$\sigma = \frac{\left(\frac{E_1}{c_1} \varepsilon_1 + \dots + \frac{E_{n-1}}{c_{n-1}} \varepsilon_{n-1}\right) + \frac{E_n}{c_n} (\varepsilon - \varepsilon_1 - \dots - \varepsilon_{n-1}) + \dot{\varepsilon}}{\frac{1}{c_1} + \frac{1}{c_2} + \dots + \frac{1}{c_n}} \quad (3)$$

Note that using the above equation, stress  $\sigma$  can be computed from state variables  $\varepsilon_1$  through  $\varepsilon_{n-1}$  and  $\dot{\varepsilon}$ . State variables satisfy the following differential equations:

$$\dot{\varepsilon}_1 = -\frac{E_1}{c_1} \varepsilon_1 + \frac{1}{c_1} \sigma, \dots, \dot{\varepsilon}_{n-1} = -\frac{E_{n-1}}{c_{n-1}} \varepsilon_{n-1} + \frac{1}{c_{n-1}} \sigma \quad (4)$$

Consequently, we can construct dynamic equation for calculating deformations of elements in the inhomogeneous beam. We repeat this for all virtual beams in the fingertip. This derivation is also exploited to model any inhomogeneous soft objects other than fingertips.

2) *Sliding Motion*: We inherited equations proposed in [10] to derive motion equations for sliding motion of the fingertip's meshed contact area. Suppose that the fingertip was pushed vertically onto a flat surface, then slid horizontally with a constant speed. Virtual beams are then deformed correspondingly, including normal and bending deformation. There are several assumptions imposed to simplify calculation:

- 1) Interactions between neighboring beams only occur among their free ends *on* the contact pad.
- 2) Only beams whose free ends are acting on the contact pad are considered. Beams outside the contact surface are insignificant to the sliding motion of the fingertip.
- 3) Nail is completely rigid and suffers no deformation during sliding motion of the fingertip.
- 4) Nail's area is always larger than the contact area.

The first and the second assumptions are important to reduce drastically calculation cost. It is because of the fact that, tissue volume of the fingertip deforms quite uniformly, while skin on the contact area can be stretched locally differently. Since superposition of beams are small and irrelevant to the precision of the model, beams deformed by pushing action do not affect beams outside the contact area, the second one is sufficient for modeling deformation of entire fingertip. If we notice Young's moduli of volumes in Table I, those of bone and nail are much bigger than that of tissue or skin. Thus the third one is also acceptable for calculation without degrade precision of the model. The last assumption is rather a reality, since most human fingertips possess a nail that covers almost upper part of the fingertip. This one allows us to eliminate beams on the contact area that make contact neither to bone nor nail, but pinned to skin.

Taking into account above assumptions, we were able to implement force calculation and motion equations. For normal force, each beam that makes contact to the flat surface possesses a deformation  $d_n^i$ . Then the external tangential force  $F_t$  starts to activate, the fingertip has not been slid yet. The contact surface still sticks to the plane, causing the fingertip to deform. At this time, all contacting beams are bent at the free ends with the same bending strain  $\delta s$ . This bending strain is calculated as originated in [13]:

$$\delta s = \frac{3\mu F_n}{16R} \frac{2-\nu}{G} \{1 - (1 - \Phi)^{2/3}\}, \quad (5)$$

where  $\Phi = F_t / \mu F_n$  is tangential force coefficient,  $R$  is fingertip's radius,  $\mu$  is friction coefficient,  $\nu$  is Poisson's ratio, and  $G$  is shear elasticity's modulus. Due to the assumption 1, bending of one inhomogeneous beam (such as beams in group N-B-S) is credited to the bending of the B-S beam. Thus its bending stiffness is calculated based on geometric quantities of the B-S beam solely.

TABLE I  
PHYSICAL PARAMETER FOR THE HUMAN FINGERTIP ([?])

	Tissue	Skin	Bone	Nail
E[Pa]	$3.4 \times 10^4$	$1.36 \times 10^5$	$1.5 \times 10^9$	$4.3 \times 10^9$
c[Pa.s]	0.1	10	1	Not used
$\gamma$	0.48	0.48	0.48	Not used

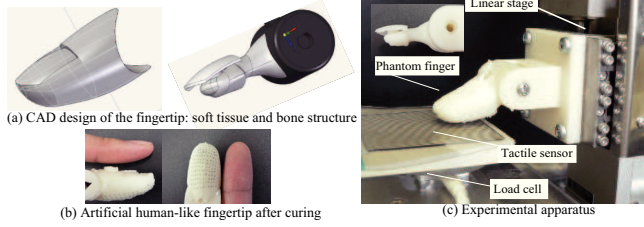


Fig. 4. CAD model of the human-like fingertip and the experimental apparatus.

For FE-based meshed contact area, there exists visco-elastic force at each contact node, which is calculated based on the node's geometrical characteristic as shown in Eq. (6):

$$\mathbf{f} = \mathbf{J}_\lambda (\lambda^{ela} \mathbf{u} + \lambda^{vis} \dot{\mathbf{u}}) + \mathbf{J}_\mu (\mu^{ela} \mathbf{u} + \mu^{vis} \dot{\mathbf{u}}), \quad (6)$$

where  $\mathbf{u}$  and  $\dot{\mathbf{u}}$  are displacement and velocity vectors of nodal points,  $\mathbf{J}_\lambda$  and  $\mathbf{J}_\mu$  are connection matrices that depend solely on geometric coordinates of nodes,  $\lambda^{ela,vis}$  and  $\mu^{ela,vis}$  are Lamé's constants that are described by Young's modulus  $E$ , Poisson's ratio  $\gamma$ , and viscous modulus  $c$ . We also introduced friction law into each node on the contact surface. Its value changes based on its contact state: stick or slip, and calculated correspondingly as follows:

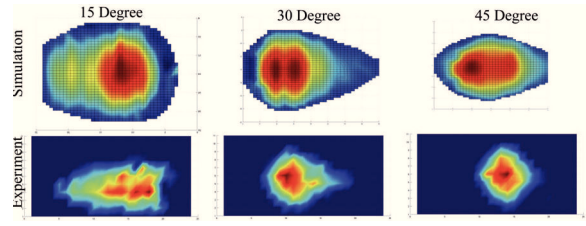
$$\mathbf{f}_{fr}^i = \begin{cases} \mathbf{f}_{ve}^i + \mathbf{f}_b^i & \text{if } \mathbf{f}_{ve}^i + \mathbf{f}_b^i < \mu \mathbf{f}_n^i \Rightarrow \text{Stick} \Rightarrow \mathbf{A}^i = \mathbf{A}_1^i \\ \mu \mathbf{f}_n^i & \text{if } \mathbf{f}_{ve}^i + \mathbf{f}_b^i \geq \mu \mathbf{f}_n^i \Rightarrow \text{Slip} \Rightarrow \mathbf{A}^i = \mathbf{A}_0^i \end{cases}, \quad (7)$$

where  $\mathbf{A}_{2,2}^i$  be a matrix to describe the constraint of the  $i$ -th node.

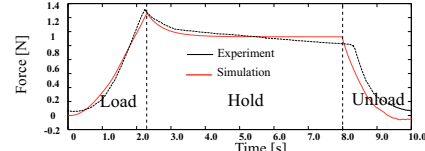
Finally, by utilizing Lagrangian formula and Constraint Stabilization Method (CSM) with a set of Lagrangian constraints  $\lambda$  and a pre-determined angular frequency  $\omega$ , we were able to construct motion equations of all contacting nodes on the contact pad as follows:

$$\begin{pmatrix} \mathbf{I} & \mathbf{0} & \mathbf{0} \\ \mathbf{0} & \mathbf{M} & -\mathbf{A} \\ \mathbf{0} & -\mathbf{A}^T & \mathbf{0} \end{pmatrix} \begin{pmatrix} \dot{\mathbf{u}}_N \\ \dot{\mathbf{v}}_N \\ \lambda \end{pmatrix} = \begin{pmatrix} \mathbf{v}_N \\ -\mathbf{K}_{ela} \mathbf{u}_N - \mathbf{K}_{vis} \mathbf{v}_N + \mathbf{F} \\ \mathbf{A}^T (2\omega \mathbf{v}_N + \omega^2 \mathbf{u}_N) \end{pmatrix}, \quad (8)$$

where  $\mathbf{M}$  is the inertia matrix of the 2-D FEA contact pad,  $\mathbf{F}$  is the vector of external forces such as bending force and friction force. This equation is linear and solvable since the matrix is regular, implying that we can compute  $\dot{\mathbf{u}}_N$ , and  $\dot{\mathbf{v}}_N$ , which are displacements and velocities of contacting nodes. Details of this derivation can be seen in [10].



(a) Normal force distribution on the contact area



(b) Dynamic response of normal force during simulated and experimental load/unload test

Fig. 5. Comparison of normal force distribution from simulation (upper row) and experiment at different contact angle. The graph shows dynamic responses of the normal force during simulated and experimented load/unload test.

### III. SIMULATION AND VERIFICATION

In this simulation, the fingertip was given a vertical push with a pre-determined contact depth, and a tangential movement with a constant velocity. Parameters used for simulation are summarized in Table I. For model's validation, we also setup an experiment similarly to that in Section II for an artificial fingertip. We have created an artificial inhomogeneous human-like fingertip based on the MRI data, with surfaces were interpolated and smoothen by computer-aided design program (see Fig. 4). The bone structure and nail were made by a 3-D printer, while the soft tissue (softness is similar to that of human tissue) were obtained after curing polyurethane rubber gel in a designed mold. By utilizing this finger, we were able to validate the proposed model precisely. In order to create movements for the fingertip, we attached it onto a 2-D linear motorized stage that can provide  $2 \mu\text{m}$ -in-resolution step.

#### A. Force-Related Results

Fig. 5(a) shows the normal force distribution when the fingertip was pushed with contact depth of 2mm and at different inclination angle of contact. We can observe that maximum force area is around the tip close to the nail, while the smaller value of normal forces are distributed mostly at the boundary of the contact surface. When the inclination contact increases, the maxima shift from right to left. Experimental results also show the similar results. As a result, it is noticeable that although outer shape of human fingertip is likely symmetrical and even, the force distribution is not produced nicely as hemispherical homogeneous fingertip case. It thanks to inner distribution of distal phalanx that causes remarkably different geometrical shapes, as well as non-uniform deformations of beams over the contact area. Fig. 5(b) illustrated one simulated dynamic load/unload test of normal force response (red solid plot). We can observe the exponentially growth/decay of the normal force during loading and unloading phase. Also the relaxation of the

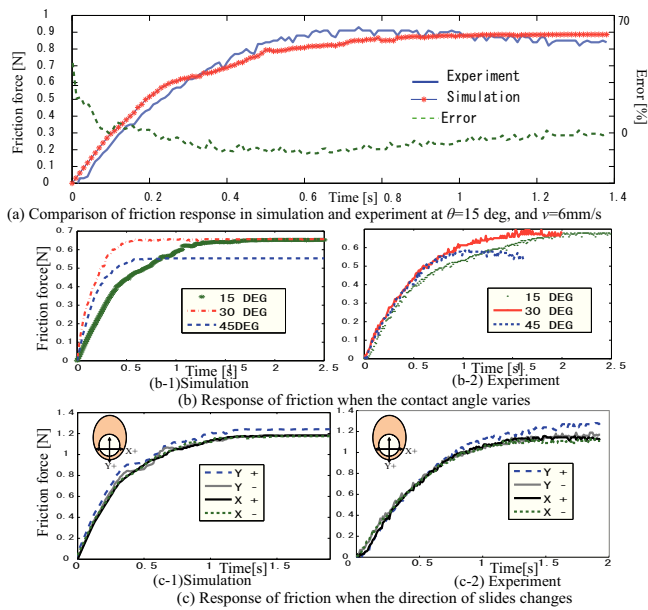


Fig. 6. Friction responses in various conditions of slide.

normal force when the fingertip was held at the given contact depth, showing a complete agreement to experimental result (black broken plot).

Fig. 6(a) plots response of friction force during stick to slip phase under constant speed. Two phases featuring change of friction force are easily observed. *Stick phase* represents pre-slide phase, when the fingertip starts to move but the contact area still sticks to the surface, *i.e.* entire movement of the fingertip has not occurred yet, in which the friction force increases remarkably (almost linear). *Slide phase* indicates the total movement of the contact area, and the friction force stays unchanged under a given speed. Fig. 6(a) also shows the agreement between simulation and experimental results, at which the error is only significant at the initial time, then reduce to less than 10% during the transition. The deflection at the simulation results was caused by artifact of numerical simulation. Plots in Fig. 6(b) indicate that when the inclination contact angle  $\theta$  varies under the same contact depth and sliding velocity, the duration time of the stick phase also change correspondingly, in which smaller angle results larger duration of the stick phase. Similar conclusion can be observed in the experiment. It is due to the fact that at small contact angle the contact area is wider, resulting more time for the localized displacement to occur, also the friction is larger at the same contact depth and sliding speed. We also investigate change at friction response when the fingertip moved in four different directions. We can observe in Fig. 6(c), in both simulation and experiment, that the friction does not vary significantly over four directions. Friction along  $Y+$  direction is always slightly larger than those along remained directions. Thus, it is difficult to judge directions of slide solely based on responses of friction.

## B. Localized Displacement Phenomenon (LDP) during Pre-Slide Phase

One of noticeable results is the success of representation of localized displacements on the contact area during pre-slide phase in simulation. Fig. 7 illustrates distribution of localized movements of contacting nodes on the contact area over time during pre-slide phase. Bright and hot color zones indicate larger movement than cold and dark color ones. These distribution were taken from the simulation of a sliding trial with sliding speed of 2 mm/s, friction coefficient of 0.7, and contact depth of 2 mm. We can observe that displacement initially occurs near the boundary of the contact area, then, along the direction of slide this movement propagates gradually. Moreover, other propagation is from outer area to inner area. As a result, this propagation of displacement relies on the normal force distribution, which indicates that small forces are distributed mainly near the boundary than the middle part (see Fig. 5(a)). The gross slide only occurs when the partial slippage exist all over the contact pad.

Fig. 7 and 8 illustrate partial movements of contacting areas in the contact pad during pre-slide phase obtained from both simulation and experiment along two distinguishing directions. While the movements of contacting points in experiment are indicated by white bars obtained from optical tracking method proposed in [11]; hot color in simulation represents larger displacement areas on the contact pad (note that the color scale is different over images.) We can observe that the propagation of slippage on the contact pad in simulation and experiment has obvious similarities in both cases. We also can assess that the propagation of localized slippage varies significantly when the fingertip slides along different directions, which is similar to conclusion mentioned in Section III-B. As a result, even response of friction over direction of slides does not vary significantly as shown in Fig. 6(c), the localized displacements act differently. This phenomenon, while complicated to detect in robotics application, is easily sensed by high density of mechanoreceptor underneath the skin in human fingertip. This is the reason why human acts so comfortably against the incipient slip of a grasped object when it tends to slip out of hand. It is a matter of fact that mechanoreceptors do not sense the change of friction force to predict the incipient slip, they are stimulated by local displacement or stretch of the skin, then tactile signals are sent to brain for processing, finally control commands are transmitted to motory system to apply more force to prevent the slippage in a real-time scenario [12]. As a result, by modeling and assessing localized displacement phenomenon, we are able to understand underlying mechanism of tactile perception of human fingertips during sliding motion.

Consequently, we have verified the BBM in an artificial human-like fingertip with a fine experimental setup. Most of sliding mechanics' characteristics of the artificial fingertip are matched with those of simulated model, such as friction and the localized displacement phenomenon.

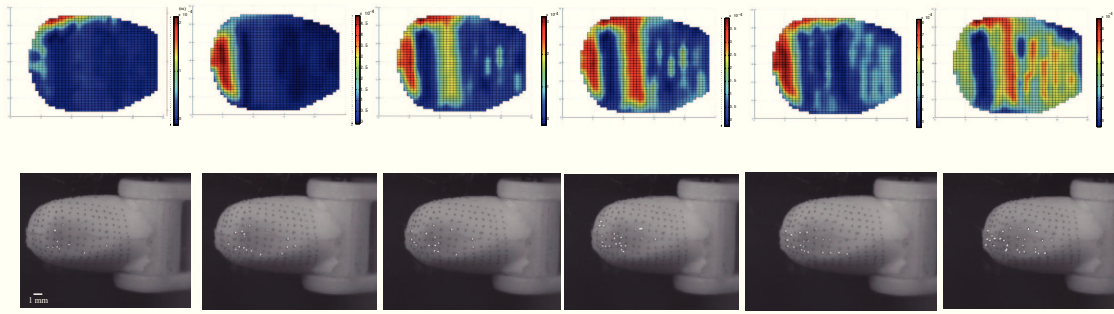


Fig. 7. Comparison in term of local displacement distributions over time when the fingertip slides along  $Y$  directions. Upper row is results from simulation.

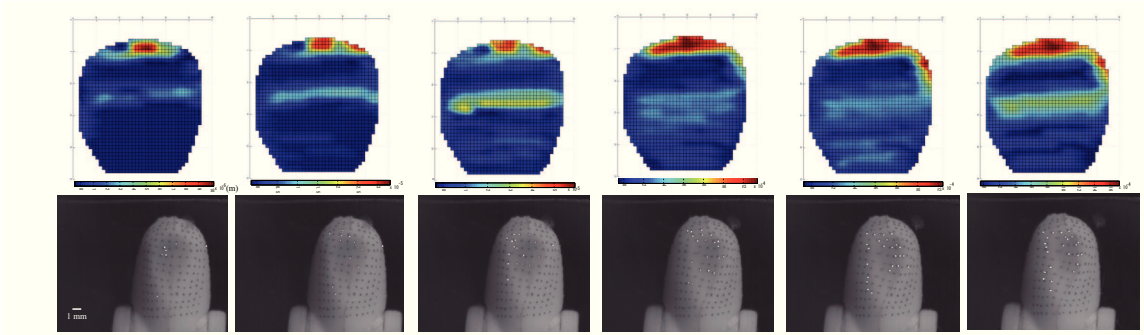


Fig. 8. Comparison in term of local displacement distributions over time when the fingertip slides along  $X$  directions. Upper row is results from simulation.

#### IV. CASE STUDY: STABLE LIFTING OF AN OBJECT

In this section, we utilized the proposed model to simulate the process of lifting an object by two fingertips of human, taking into account the change of the localized displacement phenomenon as an input. Human, when attempts to lift an object with unknown weight, pays much less effort compared to robot, thanks to condense mechanoreceptors at fingertips that can detect vibration stimulated by the slippages so that human can slightly increase grip force to stably lift it, without harm it by hard gripping. It is said by neuroscience experiments that it is skin stretch caused localized slippage on the contact with object causes those stimulation to mechanoreceptors (see [12]). Therefore, by mimicking this process with the proposed model and a simple PD (Proportion-Derivative) control, further theoretical investigation can be expedited.

##### A. Scenario

In this scenario, two identical human fingertips were approaching an object with an unknown weight. Let us assume that, for sake of simplicity, this object was a homogeneous rectangular cube. Human, with visionary assessing, could estimate where to grip the object so that two fingers were placed symmetrically on the cube's facets to eliminate unexpected rotation action (see Fig. 9(a)). Nonetheless, human cannot estimate the exact weight or fragileness of the object in order to generate suitable grip force. Therefore, he/she simply pinched the object by two fingertips (in this scenario) with a fair initial contact depth (Fig. 9(b)). Then, two

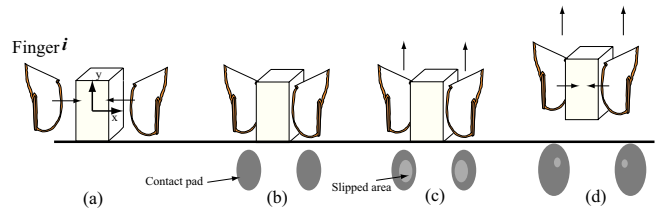


Fig. 9. Stable lifting process of human fingers.

fingertips moved up with a small velocity. During this phase, if slipped zone (indicated draftily by dark color in Fig. 9(c)) on the contact pad widened speedily, *i.e.* the object is likely to drop. Localized displacements on the contact pad expedited mechanoreceptors beneath the skin to send about-to-slip signal to human's brain. Human would increase the grip force enough to reduce the slipped area and enhance the friction in order to assure the object would not slip out of two fingers while lifting it (Fig. 9(d)).

##### B. Quantify the Slippage

To evaluate the level of slip on the contact pad, we introduced a quantitative value named as *slip indicator*  $\lambda$ , which is computed based on the ratio between the slipped area and the contact area:

$$\lambda = \frac{S_s}{S_c}. \quad (9)$$

Obviously, this indicator lies between 0, totally stick state, and 1, totally slip state. During the incipient slip, or pre-slide

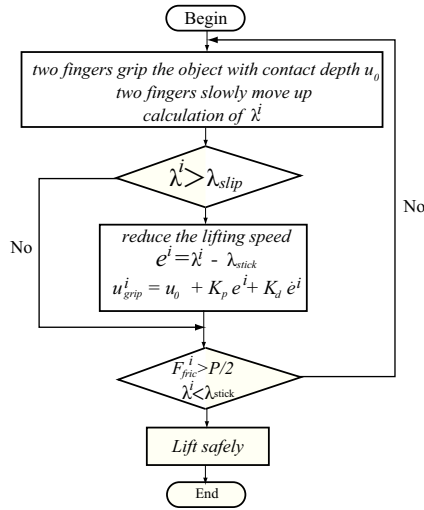


Fig. 10. Control flowchart.

phase, this ratio varies between 0 to 1. Thus, we can choose this indicator as an feedback input of current stick/slip state of the contact area between a fingertip and the object's facet. However, it is not mandatory to force this value to critical value of 0 or 1 for stick or slip state correspondingly. A small slippage can be acceptable for safe lifting, meanwhile a quick rise of the indicator, even smaller than 1, can likely cause a slippage. In this simulation, we chose the largest value for stick phase is  $\lambda_{stick} = 0.1$ , and the smallest value for slip phase is  $\lambda_{slip} = 0.5$ . These are also two important values for the control of stable object lifting simulation.

### C. Control Method

Fig. 10 illustrates the flowchart of the simulation of the stable lifting scenario. First, two fingers grip the object with a pre-determined contact depth  $u_0$ , then start to move upward gradually. In this phase, the object does not move since the generated frictions on contacts with fingers are smaller than its gravity. According to the previous sections, two fingers start to deform and the localized displacements occurs on contact areas. If the total friction ( $f_{fric} = \sum f_{fric}^i, i=1,2$ ) is not larger than the object's gravity  $P_{obj}$ , and the slip indicator of each finger  $\lambda^i$  is greater than  $\lambda_{slip}$ , say  $\lambda^i > \lambda_{slip}$  ( $i=1,2$ ), two fingers are likely to slip on the object's facets, thus a PD control is introduced to quickly increase the grip force to prevent slippages. Finally, when the total friction is larger than the object's gravity and the slip indicator falls to  $\lambda_{stick}$ , the object can be lifted safely with minimum grip force. In reality, since object's gravity is unknown, only the condition regarding slip indicator is necessary.

### D. Simulation Result

In this simulation, the object's weight was 120 gr (1.2 N), friction coefficient between fingers and the object's facets is 0.6. For the PD control,  $K_p = 3.0$  and  $K_d = 1.0$ . The initial contact depth  $u_0$  was assigned to 0.8 mm. The speed of fingers was initially accelerated gradually. When the slip

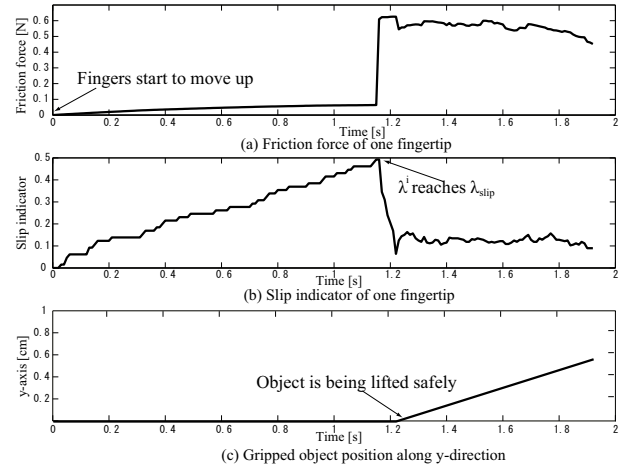


Fig. 11. Simulation result during the stable lifting.

was about to occur, the speed was decelerated to reduce the possibility of sudden drop until the stable grip was assured by the PD control. Fig. 11 shows plots obtained during the stable lifting process of human fingertips. First, two fingertips start to move upward at the initial contact depth  $u_0$ , and the object position is still unchanged. During this phase, the friction generated at one fingertip is rising up gradually, in companion with remarkable increase of the localized displacement on the contact area indicated by the slip indicator  $\lambda$  (see Fig. 11(b)). When 50% of the contact area had slipped, *i.e.*, fingertips were likely to slip out of the object's facets, the stable gripping control was activated. Two fingertips increase the contact depth simultaneously, resulting a sudden jump of the friction as well as a quick decrease of the slip indicator, assuring that two fingers did not slide on the object's facets. The PD-control law ensured the slip indicator was around  $\lambda_{stick} = 0.1$ , *i.e.* the object could be lifted up safely with the minimum gripping force. In this paradigm, we also added another condition that the total friction must be over the object's gravity 1.2 N, *i.e.* each finger's friction is over 0.6 N (see Fig. 11), before the object was lifted safely.

Consequently, the case study has shown the potential of our proposed model in studying stable grip/grasp mechanism of human soft-fingered hand. It also strengthens the selling-point that by observation of the localized displacement on the contact area, a stable grasp/manipulation can be assured with minimum grip force from human fingers. Further investigation can be developed based on our model, such as lifting irregular objects, stabilization of grasped object under disturbance, and so on.

## V. DISCUSSION

Characteristics of sliding human fingertip were successfully reflected by the BBM model, especially the localized displacements during pre-slide phase. The proposed method can act as a platform for studying sliding mechanics of sliding robotic fingertips, or inhomogeneous soft objects as a whole, in tactile perception, or creating models in

virtual environment in haptic research. One can freely introduce various friction models into contact nodes such as LuGre, Dahl [14] models other than Coulomb friction one. Also, this model is convenient to calculate *friction moment* generated through sliding motion by synthesizing partial friction moments of contact nodes to a pre-determined axis. We are planning to create a database of human fingertip, ranging from children to adult with different ages, to further investigate differences in sliding tactile mechanism, as well as enhance the proposed BBM. All codes was implemented in Microsoft Visual Studio C++ environment, in a common Personal Computer with Intel Core Duo 3.0 GHz chipset and 2.0 GB RAM. A typical dynamic simulation trial of 2 sec took about 24 minutes to complete. This is far from real-time application, but faster performance can be implemented in a GPU-equipped computer, and we are currently working toward it.

## VI. CONCLUSION

We have investigated theoretically sliding motion of a human fingertip model, focusing on pre-slide phase, utilizing proposed beam bundle model and MR images. Simulation results help us to assess the change of force, and especially localized displacement phenomenon on the contact area during pre-slide phase. Knowledge about this phenomenon will assist us to understand role of skin in recognition of slippage, as well as to develop a sensing system to detect incipient slip of human fingertip that is crucial in stable manipulation.

## REFERENCES

- [1] Mark H. Lee, *Tactile Sensing: New Directions, New Challenges*, International Journal of Robotics Research, vol. 19, no. 7, pp. 636-643, July, 2000.
- [2] A. Nahvi, J. M. Hollerback, R. Freier, and D. D. Nelson, *Display of Friction in Virtual Environments Based on Human Finger Pad Characteristics*, Proceedings of ASME Dynamic Systems and Control Division, pp. 179-184, 1998.
- [3] N. Xydias, M. Bhagavat, and I. Kao, *Study of soft-finger contact mechanics using finite analysis and experiments*, IEEE Int. Conf on Robotics and Automation, vol. 3, pp. 2179-2184, April 2000.
- [4] K. Dandekar, B. I. Raju, M. A. Srinivasan, *3-D Finite-Element Models of Human and Monkey Fingertips to Investigate the Mechanics of Tactile Sense*, Transaction of the ASME- Journal of Biomechanical Engineering, Vol. 125, pp. 682-691, Oct. 2003.
- [5] F. Barbagli, A. Frisoli, K. Salisbury, and M. Bergamasco, *Simulating human fingers: a Soft Finger Proxy Model and Algorithm*, 12th International Symposium on Haptic Interfaces for Virtual Environment and Teleoperator Systems, pp. 9-17, 2004.
- [6] S. Shimawaki, and N. Sakai, *Quasi-static deformation analysis of a human finger using a three-dimensional finite element model constructed from CT images*, Journal of Environment and Engineering, vol. 2, pp. 56-63, 2007.
- [7] M. Tada, *Individual Difference in Contact*, Journal of the RSJ, Vol. 30, No. 5, pp. 17-19, June, 2012.
- [8] I. Kao and M. R. Cutkosky, *Quasistatic Manipulation with Compliance and Sliding*, The Int. Jour. of Robotic Research, Vol. 11, No. 1, pp. 20-40, Feb., 1992.
- [9] M. Konyo and S. Okamoto, *Pseudo Haptic Representations Using Vibrotactile Stimuli*, Journal of the RSJ, Vol. 30, No. 5, pp. 23-25, June, 2012.
- [10] V. A. Ho and S. Hirai, *Understanding Slip Perception of Soft Fingertips by Modeling and Simulating Stick-Slip Phenomenon*, Robotics: Science and Systems VII, Los Angeles, CA, US, June 2011.
- [11] M. Tada and T. Kanade, *An Imaging System of Incipient Slip for Modeling How Human Perceives Slip of a Fingertip*, The 26th Annual Intl. Conf. of the IEEE EMBS, pp. 2045-2048, San Francisco, Sept., 2004.
- [12] M. J. Hertenstein, S. J. Weiss *The Handbook of Touch*, Springer Publishing Company, New York, 2011.
- [13] R. D. Mindlin, *Compliance of elastic bodies in contact*, Trans. ASME, J. Appl. Mech., vol. 16, pp. 259-268, 1949.
- [14] K. J. Astrom and C. Canudas-de-wit, *Revisiting the LuGre Friction Model*, IEEE Control Systems Magazine, Dec. 2008, pp. 101-114.